Composites: Part A 42 (2011) 1903–1909

Contents lists available at SciVerse ScienceDirect

Composites: Part A

journal homepage: www.elsevier.com/locate/compositesa

Fracture behavior and optical properties of melt compounded semi-transparent polycarbonate (PC)/alumina nanocomposites

Alexander Chandra [a], Lih-Sheng Turng [a,*], Ke Li [b], Han-Xiong Huang [b]

[a] Polymer Engineering Center, University of Wisconsin–Madison, Madison, WI 53706, USA
[b] Lab for Micro Molding and Polymer Rheology, South China University of Technology, Guangzhou 510640, PR China

ARTICLE INFO

Article history:
Received 14 December 2010
Received in revised form 18 August 2011
Accepted 20 August 2011
Available online 27 August 2011

Keywords:
A. Polymer–matrix composites (PMCs)
B. Optical properties/techniques
D. Fractography
E. Surface treatments

ABSTRACT

Low molecular weight (MW) poly(styrene-maleic anhydride) (SMA) copolymers was employed to coat spherical alumina (Al_2O_3) nanoparticles to facilitate dispersion in a polycarbonate (PC) matrix. Melt compounding was done using a high intensity thermokinetic mixer (K-mixer). The low MW SMA coating produced excellent dispersion of nanoparticles in the PC nanocomposites, resulting in fairly high light transmittance even through 2 mm thick specimens. The addition of 1 wt% well-dispersed nanoparticles improved the impact strength during brittle fracture of the PC/alumina nanocomposites through the formation of multi-level microcrazes induced by the nanoparticles. However, further increasing the alumina nanoparticle content altered the energy dissipation behavior, resulting in less effective reinforcement. Various fracture mechanisms affected by the alumina nanoparticles are presented together with the effect of thermal treatment on the PC/alumina nanocomposites.

© 2011 Elsevier Ltd. All rights reserved.

1. Introduction

Polymer nanocomposites represent a new class of lightweight, high performance materials that exhibit improved tensile strength, heat resistance, barrier properties, and/or flame retardation. Research on polymer nanocomposites has exploded in recent years, but there has been less focus on the study of spherical, non-silicate-layer-based, optical nanocomposites, especially those that utilize a melt compounding method that is capable of being scaled up. Optically transparent polymer-based nanocomposites that possess novel and tunable optical properties are suitable for a wide variety of applications such as ophthalmic lenses, view ports for armored vehicles, optical fiber sensors, optical isolators, packaging products, and medical devices.

One of the main challenges with optical nanocomposites is the requirement to retain transparency and mechanical properties. The aggregation of the nanoparticles, owing to high surface energy, could strongly hamper the optical transparency and limit the property improvement of nanocomposites. Tremendous research efforts have been devoted to stabilizing and dispersing the nanoparticles in the polymer matrices. It has been found that the degree of chemical affinity in the organic/inorganic interface is a critical factor in determining the dispersion of nanoparticles [1]. Hence, one method for facilitating the dispersion of nanoparticles is to coat the nanoparticles with a thin layer of polymer shell to introduce steric stabilization [2–9]. Such polymer coatings not only decrease the surface energy by "masking" the strong van der Waals forces of the inorganic nanoparticles, they also introduce steric repulsive forces and modify the adhesion between the nanoparticles and the polymer matrix. The resulting core–shell nanohybrids can then be readily compounded with the matrix polymer using conventional melt compounding equipment like twin-screw extruders or thermokinetic mixers.

During deformation, the ductile and brittle fracture mechanisms govern the polymer's final fracture behavior [10]. A ductile fracture is characterized by massive shear deformation around the fracture area, whereas a brittle fracture exhibits little deformation and is typically distinguished by the presence of crazes. However, it should be noted that brittle polymers such as polystyrene can also be toughened by triggering massive crazings around the deformation area through the addition of rubber fillers that cavitate during deformation [10,11]. Tough polymers typically exhibit the aforementioned deformation because they are capable of absorbing a considerable amount of energy before catastrophic failure. Other methods have also been used to improve the impact properties of polymeric materials through the addition of soft or hard particles [12–15], and the interface between the inclusion and the polymer matrix is important [14–16].

Depending on the thermal treatment (such as annealing or physical aging), PC could lose its ductility and fail in a brittle manner [17–19]. Annealing increases the yield stress and density of the polymer, thus preventing yielding and leading to brittle failure. PC

* Corresponding author. Tel.: +1 608 262 0586; fax: +1 608 265 2316.
E-mail address: turng@engr.wisc.edu (L.-S. Turng).

1359-835X/$ - see front matter © 2011 Elsevier Ltd. All rights reserved.
doi:10.1016/j.compositesa.2011.08.015

is also sensitive to defects and hence is prone to brittle failure. The main objective of this study is to examine the effects of SMA-coated spherical alumina nanoparticles on the optical and fracture behavior of PC nanocomposites that underwent two different thermal treatments (annealing and preconditioning). The light transmittance behavior of the neat resin PC and its various nanocomposites are reported, along with the impact performance, fractured surface morphology, and their correlation with existing fracture mechanics.

2. Materials and methods

2.1. Matrix and coating polymers

Optical grade Panlite AD-5503 PC resin (MFI: 64.8 g/10 min at 300 °C and 1.2 kg, Tg: 144 °C, MW: 15,000 g/mol, refractive index: 1.585) was made available by Teijin Kasei America, Inc. The SMA EF-80 (MW: 14,400, Tg: 104 °C) from Sartomer is a low MW copolymer commonly used as an additive with an 8:1 mole ratio between the styrene and the maleic anhydride.

2.2. Nanoparticles and coupling agents

Two batches of nanoscale alumina particles were used in this study. The first batch ("Batch A") of alumina nanoparticles from Nanotechnologies, Inc. had an average particle size D_{50} of 96 nm (based on the static light scattering, SLS, method) and an average specific surface area (SSA) of 50.4 m^2/g (based on the Brunauer Emmett Teller, BET, method). The second batch of nanoparticles ("Batch B") had an average specific surface area (SSA) of 57.8 m^2/g (based on the BET method). The SLS data for the second alumina nanoparticles batch were not available from the vendor although the batch was reported to have an average particle size of 30 nm. The transmission electron microscope (TEM) images in Fig. 1 provide a qualitative comparison between these two nanoparticle batches. Note that the second alumina batch (Batch B) exhibits a fairly large size distribution. Finally, fluorescamine and the coupling agent 3-aminopropyltriethoxysilane (Mw: 221.4 g/mol, SSA: 353 m^2/g) were purchased from Sigma–Aldrich and Gelest, Inc., respectively. All chemicals were used as received without further purification. Whenever necessary, drying of the nanoparticles as well as the polymer resins and composites prior to treatment/molding was performed to remove any moisture.

3. Experiments

3.1. Nanoparticle treatments

Aminosilane coupling agent and low MW SMA EF-80 were employed following the steps described in detail by Chandra et al. [7,8]. Note that during the treatment, two centrifugation processes at 2000 RPM (Batch A) and 3500 RPM (Batch B) for 20 min each were performed three times on the coated nanoparticles to remove any excess unbounded SMA EF-80. Higher RPM was used for Batch B in an effort to better collect small SMA-coated nanoparticles because of the batch's wider particle size distribution.

3.2. Nanocomposite preparation

The thermokinetic mixer (K-mixer) is a unique batch mixer that does not include any external heating elements. All of the heat required to melt the polymer results from the friction between the mixing elements, the polymer, and the surrounding wall. For preparing the various nanocomposites, the alumina nanoparticles were first hand-mixed with the PC pellets into the desired loading contents, followed by compounding in the K-mixer at 5000 RPM until the release temperature of 249 °C was reached. The typical processing time using the K-mixer was very short (in the range of 15–30 s) and the resulting hot melts were pressed into plates.

To study the possible material degradation from the thermal cycle of the K-mixer, the melt flow index, MFI, (300 °C and 2160 g) of the unprocessed PC (79.65 ± 9.96 g/10 min) and the processed PC neat resin (86.48 ± 13.30 g/10 min) were measured. The slightly increased MFI (at about 8%) suggested that the K-mixer did induce minor degradation into the polymer matrix but it is not significant. Table 1 summarizes the polymer nanocomposites produced for this study.

3.3. Characterizations

A LEO 1530 field emission scanning electron microscope (FESEM) was used to investigate the nanoparticle dispersion and the nanocomposite fractured surfaces. A Hitachi U-3010 UV–Vis spectrophotometer was employed to measure the light transmittance with wavelengths ranging from 300 nm to 700 nm. All processed PC neat resin and PC/alumina nanocomposites were hot pressed using a Carver press at 232 °C into rectangular plates using a polished mold, followed by further polishing.

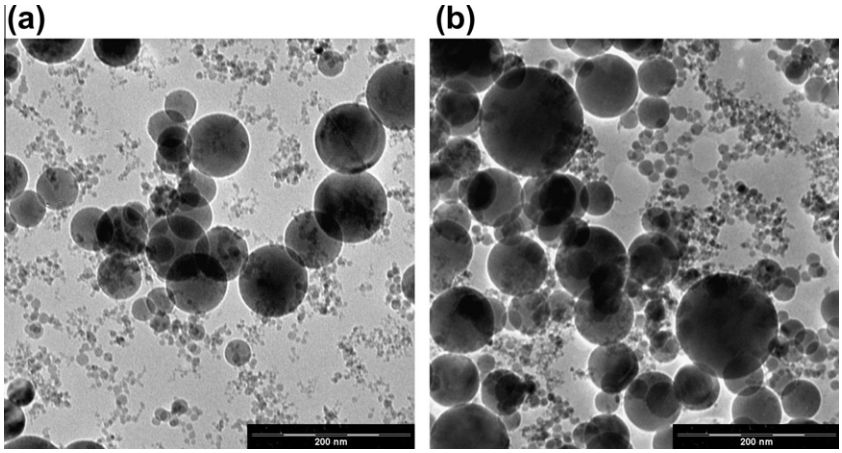

Fig. 1. TEM images of the alumina nanoparticles from different batches (left: Batch A, right: Batch B).

Table 1
The polymer/alumina nanocomposites compounded using the K-mixer and employed in the optical and impact tests and the corresponding thermal treatment.

Materials	Impact test	
	Annealed	Preconditioned
Neat PC (with one thermal cycle in the K-mixer)	✓	✓
PC with 2 wt% untreated Batch A alumina	✓	–
PC with 1 wt% SMA EF-80 treated Batch A alumina	✓	✓
PC with 2 wt% SMA EF-80 treated Batch A alumina	✓	–
PC with 1 wt% SMA EF-80 treated Batch B alumina	✓	✓
PC with 2 wt% SMA EF-80 treated Batch B alumina	✓	✓

Notched ASTM D256 Izod impact tests were performed on test bars of 50 mm by 12 mm by 2 mm with a 2.0 mm notch. At least four specimens were used for each test. Prior to impact testing, the specimens were annealed at 100 °C for 24 h for moisture removal. It was later found that this annealing process adversely induced brittle behavior in the PC. As a comparison, another set of PC neat resin and its alumina nanocomposite specimens were preconditioned at 21 °C and 50% relative humidity at atmospheric pressure for 24 h prior to impact testing to avoid inducing any brittle behavior. Table 1 summarizes the specimens used for the impact tests and the corresponding thermal treatment. Owing to the limitations of the nanoparticles, only selected nanocomposite samples were preconditioned and impact tested.

4. Results and discussion

4.1. Optical transparency

The light transmittance of representative PC/alumina nanocomposites treated with low MW SMA is presented in Fig. 2a. Note that the path length for each specimen was 2 mm thick. The light transmittance was found to be dependent on the loading content, treatment methods, the light wavelength, and the dispersion state. At first glance, higher loading content of the same batch of nanoparticles leads to reduced light transmittance, which was expected. In terms of surface treatment, untreated nanoparticles lead to reduced light transmittance due to large nanoparticle agglomerates. The effect of wavelength and dispersion state on the nanocomposites light transmittance will be discussed further in the following paragraphs.

As shown in Fig. 2a, the nanocomposites were fairly transparent at 2 mm thick, especially at larger wavelengths. Nonetheless, the nanoparticles, despite being well dispersed in the PC matrix, were still too large to totally eliminate light scattering, thereby affecting the overall transparency. The light scattering by the alumina nanoparticles was further elevated by the refractive index mismatch between the nanoparticles and polymer matrices (~1.76 for alumina versus ~1.59 for PC). Based on Rayleigh scattering criteria, dramatic light transmittance loss can only be avoided when the nanoparticle size is kept below 30 nm [20,21]. The scattered light is also inversely proportional to the wavelength of the light to the fourth power [20]. Therefore, the light scattering is more pronounced at shorter wavelengths. Fig. 2b shows the visual transparency of a 2 mm thick pure PC sample and its nanocomposite counterpart

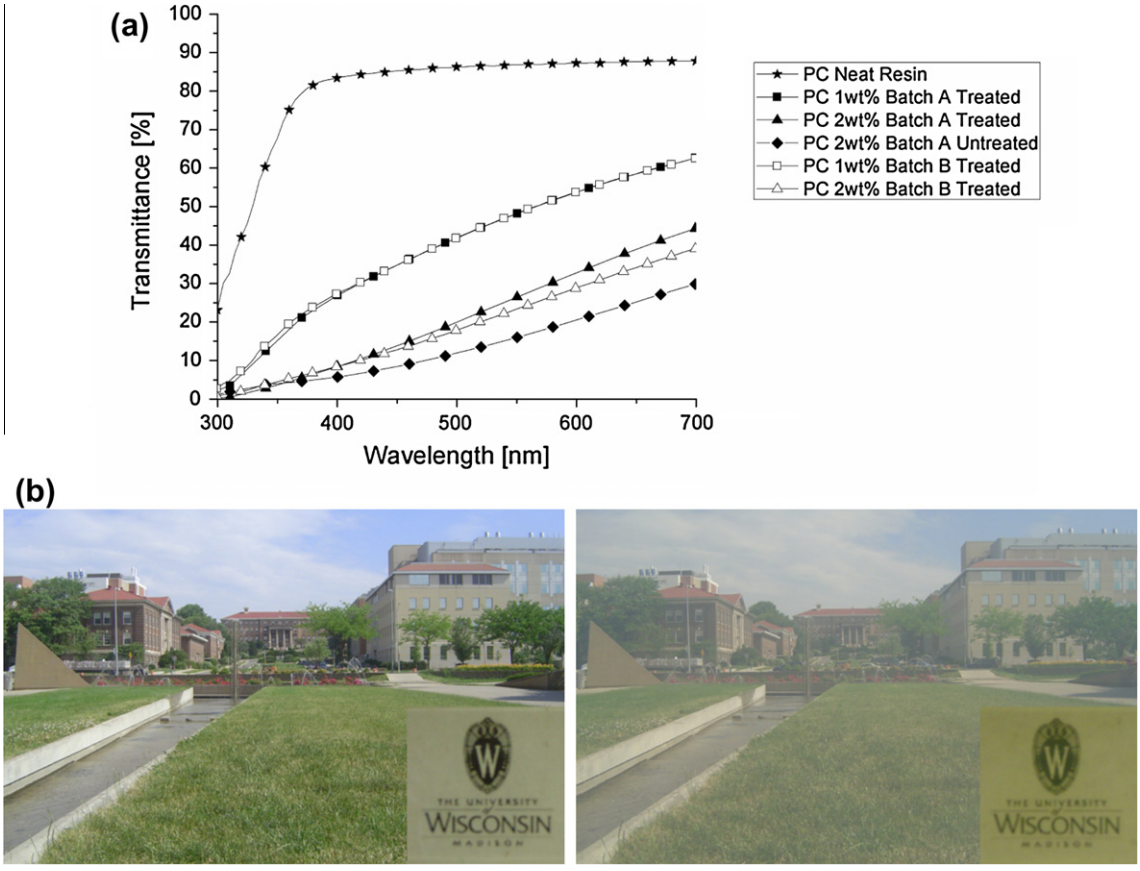

Fig. 2. (a) Light transmittance and (b) transparency of PC neat resin (left) and 1 wt% treated Batch A PC/alumina nanocomposites (right) (sample thickness: 2 mm) [8]. (For interpretation of the references to color in this figure legend, the reader is referred to the web version of this article.)

with 1 wt% SMA EF-80 treated Batch A alumina nanoparticles. The tint tone observed with the nanocomposites as shown in Fig. 2b could also be attributed to the poor light transmittance at shorter wavelengths.

Fig. 2a also shows that while the similar light transmittance behavior of the SMA EF-80 treated 1 wt% Batch A and Batch B PC nanocomposites might imply that the two nanocomposites were identical, their light scattering behavior at 2 wt% loading content was slightly different, with the 2 wt% Batch B having lower light transmittance. This will be explained in the following paragraph.

Fig. 3 shows the comparison of dispersion state between the SMA EF-80 treated 2 wt% Batch A and Batch B alumina nanoparticles. As seen in Fig. 3, the Batch B system has more individual alumina nanoparticles even though they were at the same loading content of 2 wt%. In fact, the number of particle counts, averaged from randomly selected locations but with identical sampling areas and magnification levels, for 2 wt% Batch A and Batch B were 107 ± 17 particles and 168 ± 13 particles, respectively. Since the majority of the individual alumina nanoparticles from the two batches were still larger than 30 nm, the higher nanoparticle population would contribute to the reduction of light transmittance, as each nanoparticle acted as a light scattering site.

4.2. Impact properties of annealed PC/alumina nanocomposites

The impact strengths of the annealed PC/alumina nanocomposites with various nanoparticle types, agglomerate sizes, loading contents, and prepared by various treatment methods are shown in Fig. 4. Observation of Fig. 4 suggests that during a brittle fracture (induced by annealing), the addition of alumina nanoparticles generally resulted in higher impact strengths than the PC neat resin. Furthermore, the well-dispersed 1 wt% Batch A alumina nanoparticles were capable of providing as much improvement as the 2 wt% but less dispersed (untreated) Batch A nanoparticles. However, the improvement in impact strength decreases with specimens containing well-dispersed Batch A alumina nanoparticles at a 2 wt% loading content or the well-dispersed Batch B alumina nanoparticles at 1 wt% and 2 wt%.

Various competing fracture mechanisms will be systemically presented below to elucidate the fracture behavior and shed insight into this diminishing reinforcement at higher loading levels.

Fig. 5 shows the brittle fractured surface of the annealed PC neat resin under low and high magnifications. Observation at high magnification revealed that the micro-fractured surface of the PC was smooth with no distinct features observed at the surface, which indicates the typical brittle fracture characteristics. At low magnification, the transition between stable and unstable crack propagation could be observed on the fractured surface as indicated by the transition zone line. Moreover, discontinuous crack growth was shown in the stable crack propagation region near the notch where the darker region was caused by a crack, while the lighter region consisted of multilevel microcrazes [11]. In the unstable crack propagation region on the left side of Fig. 5a, the crack traveled at a higher speed, resulting in a surface that was no longer flat [11]. Localized shear fracture could be observed as reflected by the "clam-shell" fracture. This clam-shell fracture also consisted of alternating cracks and crazes, indicated by the darker and lighter bands, respectively. The micro-fractured surface on the unstable region remained mostly smooth and the crazes on the clam-shell region consisted of single level crazes, thereby resulting in lower impact strength. Similarly, no significant energy absorption occurred in the small stable crack propagation region.

Fig. 6 shows the fractured surface of the 1 wt% well-dispersed PC/Batch A alumina nanocomposite. At low magnification, the fractured surface was flat and the transition from stable to unstable crack propagation occurred at a location much farther from the notch. Namely, the stable–unstable crack propagation transition line for Fig. 6 lies outside of the image. However, the stable crack propagation fractured surface at high magnification revealed a rough surface consisting of multilevel microcrazes. Each bright line

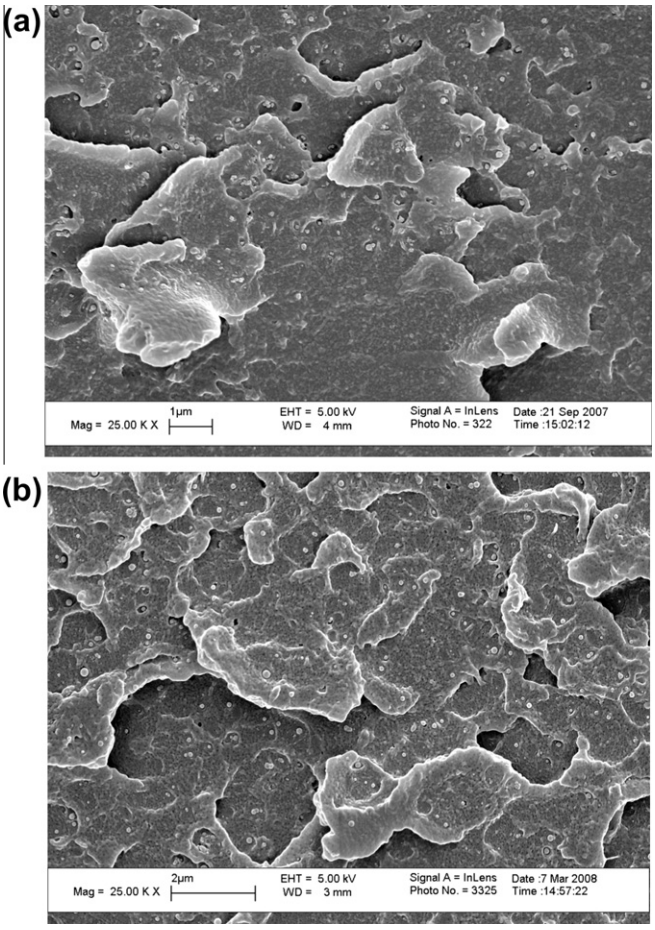

Fig. 3. 2 wt% SMA EF-80 treated PC alumina population comparison between the (a) Batch A and (b) Batch B nanoparticles.

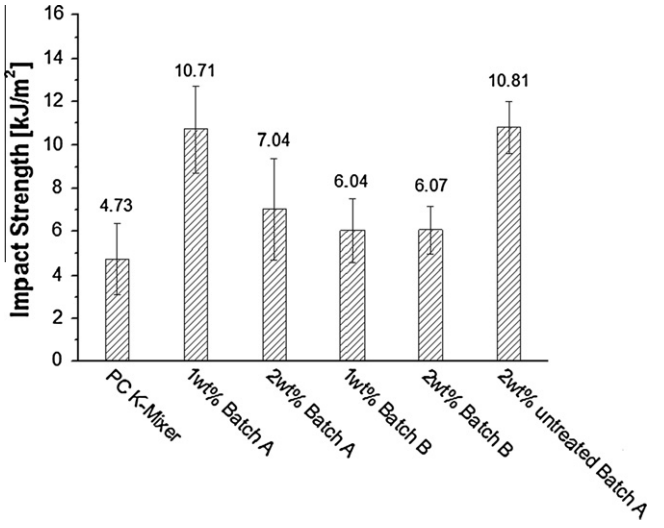

Fig. 4. Impact strength of PC neat resin (PC-K-mixer) and PC/alumina nanocomposites. For fair comparison, the neat resin went through the same thermal cycle as the nanocomposites using the K-mixer.

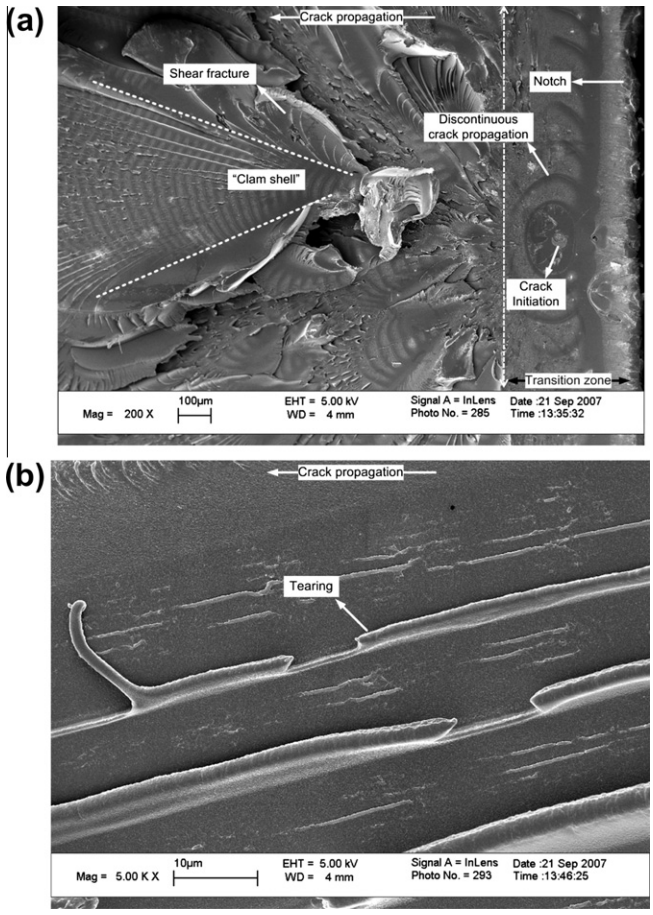

Fig. 5. Izod impact fracture surface of PC neat resin: (a) low magnification and (b) high magnification. (Dashed arrow indicates transition zone between stable and unstable crack propagation.)

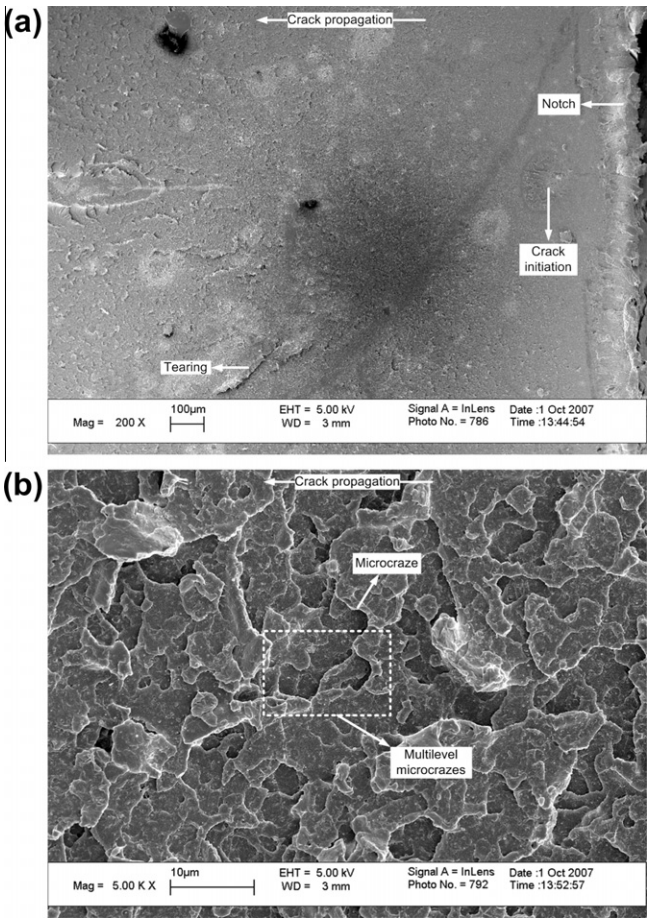

Fig. 6. Impact fracture surface of SMA EF-80 treated 1 wt% Batch A PC/alumina: (a) low magnification and (b) high magnification. (At low magnification, the white spots were surface contaminants from the environment, whereas the dark circular feature was an artifact from the FESEM.) Note that the stable to unstable crack propagation transition zone is much farther from the notch and could not be seen by the field of view for the image above.

on the micrograph depicts the coalescence of multiple fracture planes, while the dark cavity surrounded by the bright lines represents the microcrazes. During deformation, the presence of alumina nanoparticles induced void formation and craze growth. At the same time, both the voids and alumina nanoparticles also prevented the microcrazes from coalescing into a large, catastrophic crack. The multilevel fractured surface observed in Fig. 6 was formed when the nanoparticle-induced microcrazes traveled across slightly different planes and were eventually arrested. Since this microcraze formation was one of the energy dissipation mechanisms during failure, and since they occurred over a large area of the fractured surface, the PC/alumina nanocomposites were capable of absorbing more energy during failure, thereby resulting in higher brittle impact strengths than their neat resin counterparts [10,11]. Recall that the untreated 2 wt% Batch A nanocomposite had a comparable brittle impact strength improvement as the 1 wt% treated Batch A nanocomposite. The untreated 2 wt% nanocomposite also exhibited massive multilevel microcrazes during brittle impact fracture, as shown in Fig. 7, indicating a similar energy absorption mechanism.

As mentioned earlier, a higher loading of SMA EF-80 treated alumina nanoparticles in the PC matrix did not lead to further improvements in the brittle impact strength of the PC/alumina nanocomposites. The fractured surface of the well-dispersed 2 wt% Batch A alumina nanocomposite shown in Fig. 8 reveals the presence of a smaller transition zone as well as tears propagating radially from the center near the notch. The high magnification surface on the stable crack propagation region showed a combination of microcrazes and a large number of tears. These large tears implied that the additional alumina nanoparticle population altered the energy dissipation behavior and the developing microcrazes could no longer be arrested effectively, resulting in less microcrazes and thus less effective reinforcement. Similarly, the fractured surface of the well-dispersed Batch B system revealed the presence of smaller stable to unstable crack propagation transition zones. While the nanocomposites also showed similar multilevel microcrazes to the 1 wt% well-dispersed Batch A system, these multilevel microcrazes only occurred at a very small portion of the specimen stable fractured surface, and they became less well-defined as they passed the unstable crack propagation. Therefore, this reduced microcrazes formation leads to less effective energy absorption and thus reduced brittle impact strength improvement.

From the results presented above, it can be deduced that the brittle impact strength improvement of PC/alumina nanocomposites is highly dependent on the loading content, particle size and its distribution, dispersion state, surface treatment and the presence of a coupling agent and the SMA EF-80 coating. A better understanding of this interaction requires more detailed study and is beyond the scope of this paper.

4.3. Impact properties of preconditioned PC/alumina nanocomposites

The impact strengths of preconditioned Batch A and Batch B PC/alumina nanocomposites at various loading contents and their an-

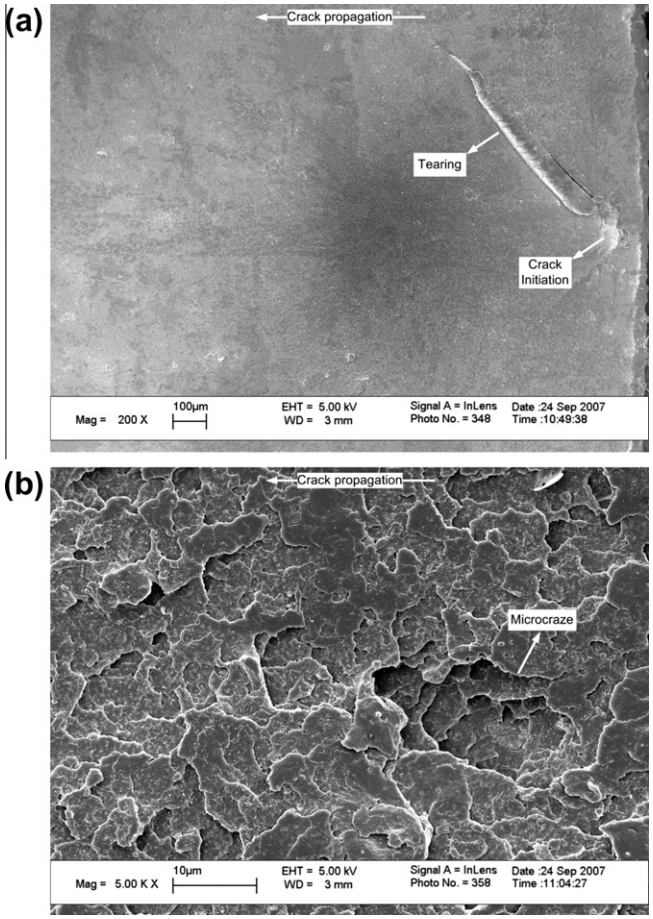

Fig. 7. Impact fracture surface of untreated 2 wt% Batch A PC/alumina: (a) low magnification and (b) high magnification. (At low magnification, the dark circular feature was an artifact from the FESEM.) Note that the stable to unstable crack propagation transition zone is much farther from the notch and could not be seen by the field of view of the image above.

nealed counterparts are shown in Fig. 9. Interestingly, the PC neat resin and the nanocomposite specimens exhibited different fracture behaviors after preconditioning and the data are more scattered with preconditioned nanocomposite samples. The preconditioned nanocomposites exhibited either ductile or brittle behavior, while the preconditioned PC was always ductile. For the 1 wt% PC/Batch A nanocomposite, 4 out of 6 specimens were ductile. For the Batch B nanocomposites, 5 out of 11 EF-80 treated 1 wt% Batch B PC/alumina nanocomposite specimens were ductile, and only 2 out of 15 specimens from the SMA EF-80 treated 2 wt% Batch B were ductile. Nevertheless, the preconditioned PC/alumina nanocomposites were similar in ductility to the PC neat resin during ductile failure. Since the PC matrix regained its ductility during preconditioning, the low nanoparticle loading content of 1 wt% and its small size were less dominant in inducing the brittle fracture, but the nanocomposites became more brittle at higher nanoparticle loading content or population. The inconsistent fracture behavior of nanocomposites could also be caused by localized nanoparticle agglomerates that occurred near the notched area (cf. Fig. 10). It is speculated that some nanoparticles could be stuck to the lid or regions in the K-mixer that could not be swept by the mixing elements or molten polymer, thereby leaving a small number of poorly dispersed nanoparticle agglomerates in the nanocomposites. The effect of these agglomerates was not a determining factor when the PC matrix was brittle when annealed but became more profound when the PC matrix regained ductility through preconditioning.

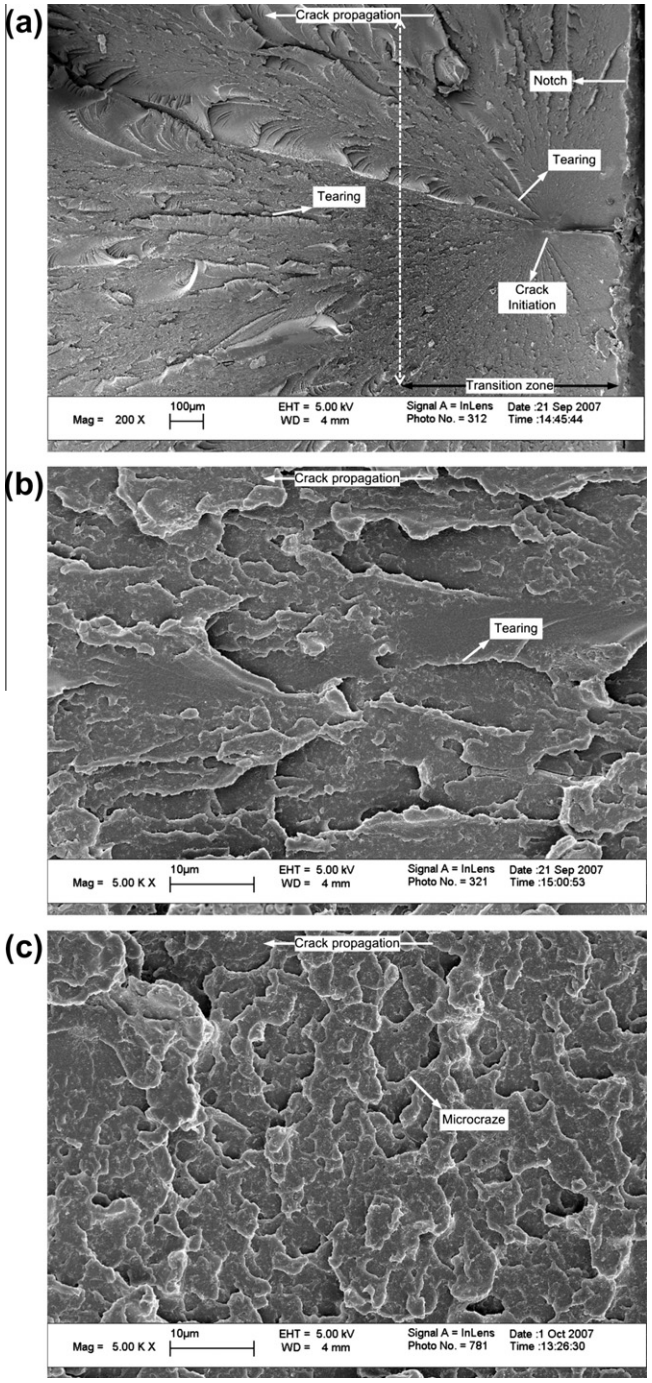

Fig. 8. Impact fracture surface of SMA EF-80 treated 2 wt% Batch A PC/alumina: (a) low magnification, (b) and (c) high magnification. (The multilevel microcrazes were only located at a small area near the notch. Dashed arrow indicates transition zone between stable and unstable crack propagation.)

5. Conclusions

Alumina nanoparticles were treated and coated with covalently bonded low molecular weight poly(styrene-maleic anhydride), SMA, and compounded with a PC matrix using a high intensity thermokinetic mixer. The combination of a low molecular weight SMA polymer coating with a high intensity mixer generated nanocomposites with excellent nanoparticle dispersion (albeit still too large individual nanoparticle size), and thus semi-transparent light transmittance was achieved even in 2 mm thick samples. In annealed PC/alumina nanocomposites, the energy absorption

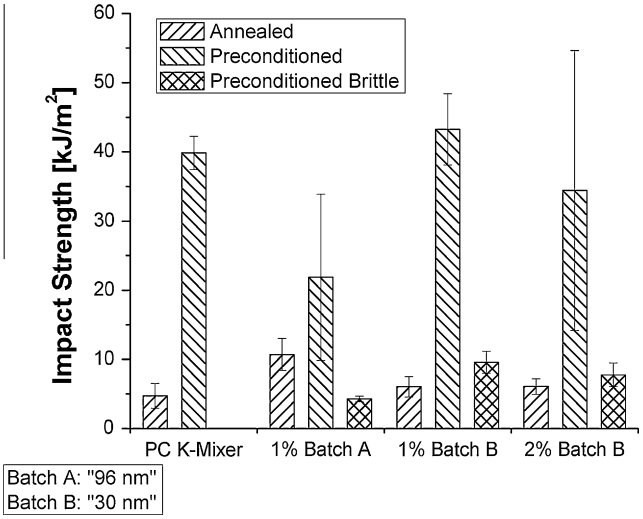

Fig. 9. Effect of thermal treatment and preconditioning on the PC neat resin and PC/alumina impact strengths. Note that the majority of the nanocomposite specimens with Batches A and B exhibited ductile fracture as shown whereas some of them fractured in a brittle fashion (see text).

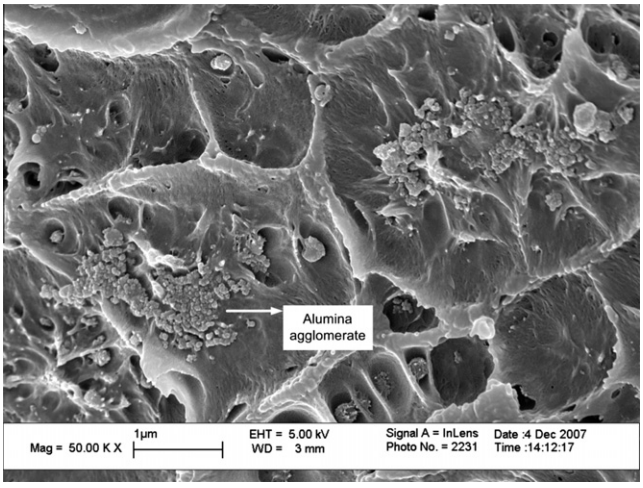

Fig. 10. Nanoparticle aggregations at the crack initiation site of the unannealed 1 wt% Batch A PC/alumina nanocomposite.

mechanism during brittle impact fracture was through the creation of multilevel microcrazes induced by dispersed nanoparticles. This enabled the nanocomposites to absorb more energy before failure, thus resulting in a higher impact strength. However, this enhancement is highly dependent to the nanoparticle size, size distribution, and population as well as the loading content which can significantly alter the fracture energy dissipation behavior. When the PC nanocomposites were preconditioned, they can exhibit either ductile or brittle fractures caused by regained ductility of the PC matrix or by the presence of localized nanoparticle agglomerates, respectively. Finally, it should be noted that the while the addition of low loading content and highly dispersed nanoparticles can lead to improved impact strength during a brittle fracture, they do not provide improvement over the ductility of nanocomposites.

Acknowledgments

The authors would like to acknowledge Professor X. Li for access to the ultrasonic mixer, Dr. Roger M. Rowell and the USDA Forest Products Laboratory (FPL) for the use of their thermokinetic mixer and lab facilities, Dr. Nelson E. Claytor from Fresnel Technologies, Inc. for providing polished molds for the samples, and Dr. Sid White of Essilor of America, Inc. for his technical assistance.

References

[1] Kelarakis A, Giannelis EP, Yoon K. Structure–properties relationships in clay nanocomposites based on PVDF/(ethylene–vinyl acetate) copolymer blends. Polymer 2007;48(26):7567–72.
[2] Cheng YR, Lu C, Lin Z, Liu YF, Guan C, Lu H, et al. Preparation and properties of transparent bulk polymer nanocomposites with high nanophase contents. J Mater Chem 2008;18(34):4062–8.
[3] Chen L, Zhu J, Li Q, Chen S, Wang YR. Controllable synthesis of functionalized CdS nanocrystals and CdS/PMMA nanocomposite hybrids. Eur Polym J 2007;43(11):4593–601.
[4] Wang Y, Zhang DS, Shi LY, Li L, Zhang JP. Novel transparent ternary nanocomposite films of trialkoxysilane-capped poly(methyl methacrylate)/zirconia/titania with incorporating networks. Mater Chem Phys 2008;110(2–3):463–70.
[5] Suo BT, Su X, Wu J, Chen D, Wang A, Guo ZH. Poly (vinyl alcohol) thin film filled with CdSe–ZnS quantum dots: fabrication, characterization and optical properties. Mater Chem Phys 2010;119(1–2):237–42.
[6] Hiemenz PC, Rajagopalan R. Principles of colloid and surface chemistry. New York: Marcel Dekker, Inc.; 1997.
[7] Chandra A, Turng LS, Gopalan P, Rowell R, Gong S. Semitransparent poly(styrene-r-maleic anhydride)/alumina nanocomposites for optical applications. J Appl Polym Sci 2007;105(5):2728–36.
[8] Chandra A, Turng LS, Gopalan P, Rowell R, Gong S. Study of utilizing thin polymer surface coating on the nanoparticles for melt compounding of polycarbonate/alumina nanocomposites and their optical properties. Compos Sci Technol 2008;68(3–4):768–76.
[9] Chandra A, Turng LS, Gopalan P. In: The polymer processing society 24th annual meeting, conference proceedings; 2008.
[10] Kinloch AJ, Young RJ. Fracture behaviour of polymers. Essex, England: Applied Science Publishers, Ltd.; 1983.
[11] Roulin-Moloney AC. Fractography and fracture mechanisms of polymers and composites. Essex, England: Elsevier Science Publishers, Ltd.; 1989.
[12] Nayak GC, Rajasekar R, Das CK. Effect of SiC coated MWCNTs on the thermal and mechanical properties of PEI/LCP blend. Compos Part A – Appl Sci 2010;41(11):1662–7.
[13] Wei GX, Sue HJ. Fracture behavior of styrene–ethylene–propylene rubber-toughened polypropylene. Polym Eng Sci 2000;40(9):1979–88.
[14] Thio YS, Argon AS, Cohen RE. Role of interfacial adhesion strength on toughening polypropylene with rigid particles. Polymer 2004;45(10):3139–47.
[15] Ash BJ, Siegel RW, Schadler LS. Mechanical behavior of alumina/poly(methyl methacrylate) nanocomposites. Macromolecules 2004;37(4):1358–69.
[16] Shah D, Maiti P, Jiang DD, Batt CA, Giannelis EP. Effect of nanoparticle mobility on toughness of polymer nanocomposites. Adv Mater 2005;17(5):525–8.
[17] Ho CH, Vu-Khanh T. Physical aging and time–temperature behavior concerning fracture performance of polycarbonate. Theor Appl Fract Mech 2004;41(1–3):103–14.
[18] Pitman GL, Ward IM, Duckett RA. Effects of thermal pretreatment and molecular-weight on impact behavior of polycarbonate. J Mater Sci 1978;13(10):2092–104.
[19] Bhardwaj R. In: Annual technical conference – ANTEC, conference proceedings; 1998. p. 2182.
[20] Althues H, Palkovits R, Rumplecker A, Simon P, Sigle W, Bredol M, et al. Synthesis and characterization of transparent luminescent ZnS: Mn/PMMA nanocomposites. Chem Mater 2006;18(4):1068–72.
[21] Bohren C, Huffman DR. Absorption and scattering of light by small particles. New York: John Wiley & Sons, Inc.; 1983.